Early View publication on www.wileyonlinelibrary.com
(issue and page numbers not yet assigned;
citable using Digital Object Identifier – DOI)

Laser Photonics Rev., 1–15 (2010) / **DOI** 10.1002/lpor.201000008

LASER & PHOTONICS
REVIEWS

Abstract Techniques used to assist phase matching of second-order nonlinearities in semiconductor waveguides are reviewed. The salient points of each method are highlighted, with their strengths and weaknesses with regard to various key applications discussed. Recent progress in these techniques is also reviewed. Emphasis is placed on two techniques, namely quasi-phase matching via domain disordering utilizing quantum well intermixing, and exact phase matching using Bragg reflection waveguides.

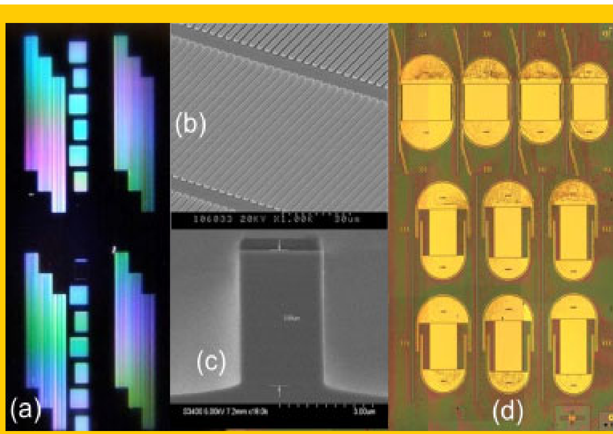

The figure shows (a) An optical microscope image of an ion implantation mask used to fabricate gratings used for quasiphase matching, (b) a scanning electron micrograph of an ion implantation mask, (c) a scanning electron micrograph of a semiconductor ridge waveguide structure, and (d) an optical microscope image of group monolithic ring lasers designed for integration with quasiphase matched structures.

Recent advances in phase matching of second-order nonlinearities in monolithic semiconductor waveguides

Amr S. Helmy[1,*], Payam Abolghasem[1], J. Stewart Aitchison[1], Bhavin J. Bijlani[1], Junbo Han[1], Barry M. Holmes[2], David C. Hutchings[2], Usman Younis[2], and Sean J. Wagner[1]

1. Introduction

The quest for harnessing optical nonlinearities began shortly after the discovery of the laser. This has been particularly the case for second-order nonlinearities, which provide distinct functionality, hence advantages for efficient frequency conversion, quantum optical applications and ultrafast all-optical signal processing [1]. In most practical cases to date, applications that use second-order nonlinear effects require constructions composed of discrete optical components and hence not necessarily amenable to integration into micro- and nano-fabricated settings. However, monolithic integration could fuel wider adoption and utilization of these technologies. Most nonlinear optical crystals do not lend themselves to the nano-fabrication technologies available for semiconductors, which enable more advanced functionality such has high-Q cavities, photonic bandgap and quantum confinement effects, among others. Materials that do have an appreciable nonlinearity don't have the phase-velocities of the interacting harmonics matched naturally, leading to inefficient interaction [2]. This is mainly due to dispersive effects which are associated with operating at wavelengths that are in the vicinity of material resonances. Phase matching the phase velocities of the interacting waves has been mastered in several material systems such as periodically poled lithium niobate (PPLN) [3], potassium titanate phosphate (KTP) [4] and barium borate (BBO) [5], where techniques such as birefringence phase matching and quasi-phase matching (QPM) have been used to achieve efficient optical sources, ultrafast optical processing elements and frequency conversion components [6–8]. However, phase matching proves more difficult in semiconductors. If achieved effectively it can enable the use of the large second-order nonlinearity in conjunction with the broad base of optoelectronic devices already developed for this platform.

Phase matching in semiconductors was achieved in materials such as ZnTe and ZnSe in 1995 [9, 10]. For GaAs it was achieved initially in 1992 [11] and for InP also in 1992 [12]. The nonlinearity of semiconductor materials is generally larger than that of their most common nonlinear crystal counterparts such as KTP, PPLN and BBO while operating near material resonances. This benefit is often offset by the enhanced optical losses in semiconductors operating in this regime [13–15]. GaAs- and InP-based material systems, despite having higher propagation losses in comparison to other nonlinear crystals, have a well-developed platform, where lasers, modulators, amplifiers,

[1] The Edward S. Rogers Sr. Department of Electrical and Computer Engineering, University of Toronto, 10 King's College Road, Toronto, Ontario M5S 3G4, Canada [2] Department of Electronics and Electrical Engineering, University of Glasgow, Glasgow G12 8QQ, UK
[*] Corresponding author: e-mail: a.helmy@utoronto.ca

photonic bandgap structures and other devices have been developed [16–20]. In the case of GaAs compounds, the transparency window is between 0.9 and 17 µm, compared to between 0.5 and 5 µm for lithium niobate [21]. GaAs compounds also have higher optical damage thresholds. The integration of second-order nonlinearities with these devices offers distinct functionality and advantages, and hence driven a great deal of research for efficient phase matching in these material systems.

2. Second-order nonlinearities in semiconductors

The most generic second-order nonlinear optical process is three-wave mixing. For this process to occur, the participating waves must satisfy the energy conservation relation $\omega_3 = \omega_1 + \omega_2$. With two input waves, two interactions from this are possible: sum frequency generation and difference frequency generation (DFG). With a single input wave, $\omega_1 = \omega_2$ at the degeneracy point, second harmonic generation (SHG) can take place. Also, by launching only ω_3, spontaneous parametric downconversion (SPDC) is possible, where photons at ω_1 and ω_2 are generated. The strength of the interaction is determined by the magnitude of the second-order nonlinear susceptibility $\chi^{(2)}$. However, second-order processes also require that the interacting waves be 'phase matched' such that the propagation constants satisfy the momentum conservation relation $k_3 = k_1 + k_2$, where $k_i = n_i\omega_i/c$ $(i = 1,2,3)$, in which n_i are the refractive indices of the interacting waves and c is the speed of light in a vacuum. If the three waves travel in the same direction and their refractive indices are identical, the phase-matching condition is automatically satisfied since $\omega_3 = \omega_1 + \omega_2$. In this case, energy conservation ensures phase matching. However, since all materials are in reality dispersive, the three waves actually travel at different velocities corresponding to their different refractive indices, n_1, n_2 and n_3. The phase-matching condition becomes $n_3\omega_3 = n_1\omega_1 + n_2\omega_2$, which is independent of energy conservation. Both conditions must be simultaneously satisfied. Precise control over the refractive indices for the three frequencies is required for exact phase matching. This can be achieved, for example, by appropriate selection of the polarization in conjunction with control of temperature or angle of propagation. Because semiconductor materials show significant dispersion, and do not lend themselves to birefringence phase matching, their phase matching can be challenging. QPM involves compensating for the phase velocity mismatch between the interacting waves, which in turn controls the power flow between them. In the case of QPM, for a SHG process, the pump wave (ω_3) generates a second harmonic wave (ω_1) upon passing through a medium with quadratic nonlinear susceptibility. Due to the phase mismatch between them, the pump and second harmonic waves accumulate a phase shift of π over a distance known as the coherence length, $l_c = \pi/(k_3 - 2k_1) = \lambda_3/4(n_3 - n_1)$, where λ_3 is the vacuum wavelength of the pump. The direction of power flow between the fundamental and harmonic depends on the relative phase of both waves, and hence changes sign every coherence length. By changing the sign of the nonlinear susceptibility every coherence length, the phase of the polarization wave is shifted by π, effectively rendering the power transfer to be unidirectional with length. This in turn leads to monotonic power flow into the second harmonic wave (as illustrated in Fig. 2).

GaAs and related compounds possess the zinc-blende (cubic) structure which has $\bar{4}3$m symmetry. This symmetry group does not possess inversion symmetry and has an inherent second-order optical nonlinearity. However, cubic structures have isotropic linear optical properties and therefore lack birefringence. Thus, second-order nonlinear processes require another means of phase matching. Epitaxial layers of these compounds are usually grown on GaAs substrates along the [001] plane and are cleaved along [110] planes. In bulk layers, these materials possess one independent second-order tensor element $\chi^{(2)}_{xyz}$ and overall six elements [22]. The other elements are those where the coordinates have been interchanged with all permutations. It should be noted that the additional tensor elements $\chi^{(2)}_{zxx}$, $\chi^{(2)}_{xzx}$ and $\chi^{(2)}_{zzz}$ can be obtained using quantum confined heterostructures to break the crystal symmetry. Phase matching via periodic modulation of these structures has been demonstrated; however, the effect was found to be too small to be useful [23].

In rectangular guided wave crystalline semiconductor structures, and in particular in the AlGaAs material system, the participating waves are typically guided along the [110] direction. The boundary conditions in the waveguides result in modes of the transverse-electric (TE) type polarized along [110] and the transverse-magnetic (TM) type polarized along [001]. Given the considerations discussed above, there are predominantly two configurations of phase matching for these waveguides: (1) type I phase matching and (2) type II phase matching. In type I, ω_3 is TM polarized, and ω_1 and ω_2 are TE polarized. In type II, ω_3 is TE polarized and one of either ω_1 or ω_2 is TE polarized while the other is TM polarized. For the specific case of SHG, the type I configuration produces a TM-polarized second-harmonic wavelength for a TE-polarized fundamental wavelength, while type II phase matching yields a TE-polarized second harmonic for a hybrid TE/TM fundamental.

3. Phase-matching techniques in semiconductor waveguides

Numerous techniques and associated waveguide structures have been investigated over the last two decades to phase match second-order nonlinear processes. In general, the phase-matching methods can be grouped as either exact phase matching (EPM) methods or QPM methods. For EPM, we review form-birefringence phase matching (FBPM) and modal phase matching (MPM). Several QPM methods are also reviewed, including our work with domain-disordered quasi-phase matching (DD-QPM) which is discussed in detail in Sect. 4.

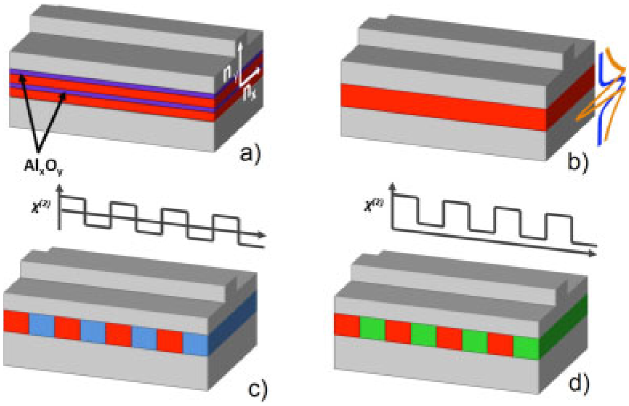

Figure 1 (online color at: www.lpr-journal.org) Waveguide structures for a) form-birefringence phase matching, b) modal phase matching, c) domain-reversal quasi-phase matching and d) domain-disordered quasi-phase matching.

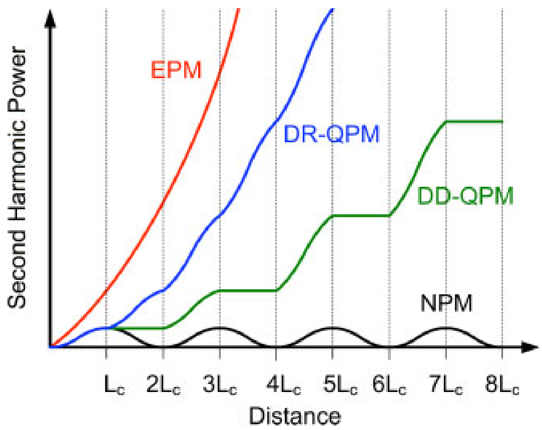

Figure 2 (online color at: www.lpr-journal.org) Comparison of exact phase matching (EPM), domain-reversal quasi-phase matching (DR-QPM) and domain-disordered quasi-phase matching (DD-QPM) over intervals of the coherence length for the SHG process. Nonphase-matched (NPM) SHG is also shown.

3.1. Form-birefringence phase matching

The primary obstacle to achieving phase matching in AlGaAs is the lack of birefringence as a natural material property. However, a multilayered structure can be engineered to provide an artificial form-birefringence. As shown in Fig. 1a, such FBPM waveguides can be fabricated in AlGaAs by incorporating thin aluminum oxide (AlOx) layers in the waveguide core. This is usually achieved via the oxidation of AlAs. The large refractive index difference between the AlGaAs ($n = 3.3$) and AlOx ($n = 1.6$) layers is sufficient to induce similar effective indices for the TE and TM modes of different wavelengths allowing EPM to be achieved. The AlOx layers are realized by selective oxidation of high aluminum content AlGaAs layers originally grown into the structure by epitaxy. All other AlGaAs layers remain as intact crystals with their nonlinear properties preserved. This technique is attractive because no wafer bonding, oxide deposition or regrowth is required. As the AlOx layers are thin, significant overlap of the optical mode is maintained with the highly nonlinear AlGaAs layers. Tuning of the phase-matching wavelength can be achieved by changing the waveguide ridge width. Several groups have used AlGaAs/AlOx waveguides to demonstrate SHG [24], DFG [25], parametric fluorescence [26], resonantly enhanced SHG [27] and parametric amplification [28].

While several devices have been demonstrated, FBPM waveguides have several issues to be resolved. Firstly, linear losses are significant ($> 20\,\mathrm{dB\,cm^{-1}}$) for both the fundamental and second-harmonic wavelengths. This is primarily due to the amorphous AlOx layers and roughness at the interfaces between the AlOx and AlGaAs layers. Secondly, FBPM devices have been reported to have low damage thresholds, which is likely to be because of the presence of defect states at the AlOx interfaces which leads to excessive absorption and heating. Thirdly, integrating active devices would be a considerable challenge given that AlOx is electrically insulating and thus a barrier to current injection for lasers. Furthermore, even the presence of unoxidized high aluminum content layers presents a challenge to the process of including dopants to form p-type and n-type material for a laser diode. Lastly, the oxidation of these devices is complex requiring tight control over the process parameters.

3.2. Modal phase matching

EPM can also be achieved in semiconductor waveguides by using the technique known as MPM. In this method, a multimode waveguide structure is designed such that the fundamental modes of one or two of the wavelengths in the three-wave mixing processes are phase matched with a higher order mode of the other wavelength, as shown in Fig. 1b. The longer wavelengths are further away from the bandgap resonance in the material index and tend to have lower effective indices at shorter wavelengths. Since the effective index of a waveguide tends to decrease as the mode order increases, it is the shortest wavelength of the process (the second harmonic in SHG, the pump in DFG) that propagates in a higher order mode. SHG by MPM has been demonstrated in AlGaAs waveguides at wavelengths around 1550 nm using a femtosecond pulsed source [29] and using a continuous-wave source [30] with output second-harmonic powers in excess of 1 μW.

MPM does have some limitations. Losses generally increase with higher order modes. The shorter wavelength, which already has a higher Rayleigh scattering loss with the sidewall roughness and absorption loss due to proximity to the bandgap energy, would experience more radiation loss due to reduced confinement. Furthermore, bend losses would be larger for higher order modes which limit the potential for integration with devices with curved waveguides such as ring resonators. The overlap area between the low- and high-order modes involved in the mixing process is also of concern. The variation of the phase across the profile of the higher order modes as well as the dissimilar mode distribution with respect to the fundamental, limits the interaction between the modes and reduces conversion efficiency. Higher order modes are also more difficult to exploit due to their irregular diffraction patterns, the efficient collection and focusing of which are challenging.

3.3. Quasi-phase matching

The alternative to EPM is QPM. In this technique, the participating waves are allowed to propagate in a nonphase-matched fashion. The phase mismatch accumulated is periodically corrected along the length of the waveguide by modulating $\chi^{(2)}$ at intervals of the coherence length L_c, thus forming a $\chi^{(2)}$ grating. In the domain-reversal QPM (DR-QPM) technique, $\chi^{(2)}$ is alternated in sign from positive to negative. Such a structure is depicted in Fig. 1c. In the SHG process, this results in a quasi-continuous power transfer to the generated wave as shown in Fig. 2. In another QPM method, referred to here as domain-suppressed QPM (DS-QPM), the magnitude of $\chi^{(2)}$ is periodically suppressed such that it alternates between regions of high nonlinearity and low nonlinearity, as depicted in Fig. 1d. Power is transferred to the second-harmonic wave in regions where the high nonlinearity remains intact. The regions in which $\chi^{(2)}$ is suppressed produce little or no back conversion to the fundamental wave, only allowing the waves to realign in phase before encountering the next high-nonlinearity region. As a result, power is transferred in a stair-step pattern with each step being two coherence lengths. In both methods, the phase-matching wavelength is determined by the period and duty cycle of the grating. All things being equal, QPM by either technique does not result in as much power transfer per unit length as EPM techniques. Furthermore, the coherence lengths in AlGaAs-based semiconductors can be less than 2 μm, which presents a challenge to the fabrication processes. Often, high-order gratings are necessary to meet the resolution limitations. However, the magnitude of $\chi^{(2)}$ in semiconductors is large, and as a result, conversion efficiencies in semiconductor QPM devices can potentially exceed those of bulk crystals used in EPM. Losses are also potentially lower than those of form-birefringence waveguides, allowing longer waveguides and higher conversion.

DR-QPM has been achieved in AlGaAs waveguides by, for example, periodically rotating the orientation of the crystal by 90° about the $\langle 001 \rangle$ crystal axes. The rotated anti-phase domains have a $\chi^{(2)}$ value opposite in sign to the normal domains, which is equivalent to shifting the relative phase of the waves by 180°. Creating rotated domains was initially achieved by one of two methods: (1) wafer bonding and (2) orientation-patterned regrowth. In the former, a grating pattern is etched into two different wafers, with one wafer oriented 90° relative to the other. That wafer is then flipped over and aligned with the other wafer such that the gratings fit into each other. The substrate of the flipped wafer is then etched off and ridge waveguides are formed by lithography. Yoo et al. used this fabrication technique with AlGaAs waveguides to demonstrate SHG [31] and DFG [32]. While this technique has shown some success, the etching and wafer bonding leads to rough and uneven interfaces between grating domains leading to high scattering losses. To address this issue, a method based on regrowth on patterned substrates has been developed. In this technique, the QPM grating pattern is defined lithographically, then transferred into a few monolayers of overgrown Ge on the starting material followed by regrowth of the same material. The regrowth leads to a crystalline structure with different phase orientations depending on whether the growth takes place on the original substrate or on the Ge layer. Orientation-patterned GaAs (OP-GaAs) has been used to demonstrate SHG [33], SHG from a mid-IR source [34], mid-IR continuum generation [35] and a terahertz source [36]. While this method of fabrication has the advantage of reducing scattering losses at the domain interfaces, complete bonding of the crystalline structure cannot be achieved due to the anti-phase orientation of the lattice, which ultimately leads to scattering. Furthermore, roughness at the interfaces introduced during the reactive-ion etching process results in high losses. Also, any misalignment of the core layer in the regrown material can lead to mode profile oscillations and the formation of an effective index grating. Progress has been made recently to reduce the scattering loss by reducing the corrugations of the domains resulting from original template and regrowth processes [37–39]. Minimum losses of 4.5 dB cm^{-1} at 1.55 μm and 9.7 dB cm^{-1} at the second-harmonic wavelength were obtained, and the highest internal conversion efficiency of 43% W^{-1} was achieved in an 8 mm long waveguide under continuous-wave operation [38, 39]. Optical parametric oscillators in QPM OP-GaAs pumped by differently polarized pulses were also demonstrated [40, 41]. With a pump pulse duration of 26 ns and wavelength of 2.79 μm, optical parametric oscillator (OPO) thresholds of 30, 29 and 50 μJ were obtained for [111] linearly, circularly and depolarized pumps, respectively [41]. A threshold of 100 nJ was achieved for a pump with pulse duration of 1 ps at 3.3 μm wavelength [42]. Furthermore, a tunable terahertz wave was generated by down-conversion in OP-GaAS when combined with a PPLN OPO cavity [36, 43].

Domain suppression can also be achieved by altering the material composition along the waveguide. In the case of AlGaAs, higher aluminum content results in a lower $\chi^{(2)}$ value since the bandgap energy is shifted to lower wavelengths. In one method of DS-QPM, a grating is etched and the removed material is replaced with one having a different value of $\chi^{(2)}$. While DS-QPM is less efficient over length compared to DR-QPM, as depicted in Fig. 2, it can be achieved without encountering the anti-phase interface problem, which reduces scattering losses. The advantage of using AlGaAs over other materials is the lattice match across all Al mole ratios, which ensures minimal regrowth defects. Unlike DR-QPM, each domain has the same crystal orientation and smoother domain interfaces are achievable. Lastly, the fabrication method is technologically simpler than that for OP-GaAs since it involves fewer processing steps. Rafailov et al. [44] formed such a QPM grating by periodically replacing the originally grown GaAs waveguide core layer with regrown $Al_{0.4}Ga_{0.6}As$. However, while per-

LASER & PHOTONICS REVIEWS

Table 1 Comparison of efficiencies obtained for various samples using different phase-matching techniques. (FBPM, form-birefringence phase matching; CEBPM, cavity-enhanced birefringence phase matching; WBQPM, wafer bonding quasi-phase matching; OPQPM, orientation-patterned quasi-phase matching; DDQPM, domain-disordered quasi-phase matching; MPM, modal phase matching; BRW, Bragg reflection waveguide.)

Sample	Technique	P_p (mW)	P_SH (μW)	L (mm)	η ($\%\mathrm{W}^{-1}$)	η_norm ($\%\mathrm{W}^{-1}\mathrm{cm}^{-2}$)	Pump wavelength (μm)	Pulse duration	Ref.
GaAs/AlOx	FBPM	5	1.3×10^3	1.0	5200	5.2×10^5	2.01	200 fs	[24]
GaAs/AlOx	FBPM	1.1	2.3	1.7	190	6.6×10^3	1.61	8 ps	[65]
GaAs/AlOx	CEBPM	–	1.4×10^{-4}	0.6	4–5	$1.1–1.4\times10^3$	1.55	cw	[27]
AlGaAs	MPM	20	10.3	1.5	2.5	111	1.54	250 fs	[29]
AlGaAs	MPM	0.9	5.8×10^{-3}	1.5	0.7	30±5	1.55	cw	[30]
AlGaAs	BRW	3.3	60	2.2	551	1.1×10^4	1.55	1.8 ps	[66]
GaAs	WBQPM	–	–	3.0	4.9	54	1.466	cw	[31]
GaAs	OPQPM	7.8	4.8	8.0	43	67	1.56	cw	[38]
GaAs	DDQPM	84	1.6	3.5	0.022	0.18	1.546	cw	[67]

fectly crystalline interfaces are possible, scattering between domains is still unavoidable due to the deep-etching process creating rough interfaces. Furthermore, the regrowth process invariably leads to misalignment of the core layers, as with the DR-QPM techniques. An obstacle still persists, however, which is due to the refractive index difference between the different layers with dissimilar Al concentrations. This leads to an unavoidable refractive index grating that subsequently leads to excess scattering losses.

The concept of QPM has proven to be very useful in order to enhance nonlinear conversion. Recently, there has been some interest for resonant SHG in Bragg multilayers, also called finite one-dimensional photonic crystals [45–57]. Strong enhancement of SHG takes place when the pump and/or harmonic waves are resonant with band-edge states that are formed in the finite structure. In particular, phase matching occurs when the pump beam is tuned to the first band-edge resonance of the mth-order stop band and the harmonic beam is tuned to the second resonance of the $2m$th-order stop band [48]. Finally, the combination of both phase matching and high electromagnetic field confinement leads to giant conversion efficiencies. Under these conditions, SHG efficiency has been shown to scale as N^6, where N is the number of periods [49]. Experimentally, scaling faster than N^5 has been demonstrated in $\mathrm{Al}_x\mathrm{Ga}_{1-x}\mathrm{As}$/AlOx multilayers [50]. Moreover, N^8 scaling of SHG efficiency has been obtained when the pump and harmonic waves are both tuned to the first band-edge resonances at the second to fourth stop-band edges, in a situation when phase-matching conditions are not fulfilled [57].

Besides using Bragg gratings, phase matching can also be achieved by using local defect modes within the forbidden band [58–60] and introducing corrugations in thin-film waveguides [61]. Two-dimensional photonic crystal structures have also attracted some interest due in part to the relative ease of working at sub-micrometer length scales, and because they are directly compatible with the extensive waveguide-based optoelectronics industry [62, 63]. Unlike one-dimensional photonic crystals where the phase-matching conditions can be reached in specific propagation directions only, the application of two-dimensional photonic crystals can allow phase matching in all propagation directions [64].

A summary of the recent and most notable results for SHG based on GaAs using different phase-matching technologies and different pump pulse durations is given in Table 1. SHG is used as a comparative point for each technology due to the availability of results. The efficiencies used for comparison are defined as follows. For type I, the overall conversion efficiency $\eta = P_\mathrm{SH}/P_\mathrm{p}^2$, where P_p and P_SH are pump and generated second-harmonic powers, respectively, and the normalized conversion efficiency $\eta_\mathrm{norm} = P_\mathrm{SH}/(P_\mathrm{p}^2L^2)$ which normalizes the conversion efficiency by the sample length L. For type II, $\eta = P_\mathrm{SH}/(4P_\mathrm{p}^\mathrm{TE}P_\mathrm{p}^\mathrm{TM})$ and $\eta = P_\mathrm{SH}/(4P_\mathrm{p}^\mathrm{TE}P_\mathrm{p}^\mathrm{TM}L^2)$, where P_p^TE and P_p^TM are TE and TM components of the pump powers, respectively.

4. Domain-disordered quasi-phase matching

The challenges of the QPM methods mentioned are numerous, hence the pursuit of other solutions. Achieving lower loss is necessary for efficient conversion, and thus there is a need to simplify the fabrication process. There is also a need to integrate QPM structures with other optical devices, requiring that the fabrication processes allow this with ease and flexibility. We have been working on an approach to DS-QPM using a post wafer growth process known as quantum well intermixing (QWI) [68]. This approach has several advantages over EPM and other QPM methods, most notably its simplicity and greater integration possibilities. In this section, we review our work on DD-QPM waveguides.

4.1. Quantum well intermixing

In QWI, a quantum well structure is used as the core of the waveguide. The sample is subjected to one of several processes such as ion implantation, to introduce point defects into the semiconductor crystal lattice. The sample is then heated to a high temperature by rapid thermal annealing (RTA) which allows the lattice atoms to diffuse, a process promoted by the presence of the defects. This diffusion process has the effect of both repairing the crystal lattice and of altering the composition and structure of the quantum wells. As a result, the optical properties, such as the absorption/emission bands and refractive index are modified. QWI has been used successfully as a means to blueshift the absorption band in lithographically defined regions. This allows pump lasers to be mixed with passive optical components. However, the intermixing process has also been shown to alter the nonlinear optical properties of the quantum well structure [69]. Furthermore, the absorption/emission band and nonlinear strength can be manipulated with varying degrees of intermixing on the same chip [70], opening the possibility of monolithic integration of complex photonic integrated circuits and systems.

There are two possibilities for suppressing $\chi^{(2)}$ to form a QPM grating. In the first, referred to as the symmetry modulation technique, an asymmetric quantum well (AQW) structure is used as the starting material. The structural asymmetry induces additional $\chi^{(2)}$ tensor elements not ordinarily found in bulk zinc-blende semiconductors. Those elements vanish during QWI as the material reverts to a more symmetric structure. In the second method for suppressing $\chi^{(2)}$, referred to here as the bandgap modulation technique, QWI causes the quantum wells to broaden and become shallower. This increases the energy bandgap and thus shifts the dispersion curves of the optical properties (such as the refractive index and the nonlinear susceptibilities). By operating at wavelengths near the half-bandgap energy of the starting (or 'as-grown' material) $\chi^{(2)}$ can be significantly suppressed as the $\chi^{(2)}$ resonance peak at this energy is shifted to shorter wavelengths. Using either method, QPM gratings can be formed by periodically intermixing the quantum well structure to suppress $\chi^{(2)}$ [71]. As such, this technique is known as DD-QPM. The key advantage of this method is that it does not require etch-and-regrowth processes and has the potential for creating smooth and defect-free domain interfaces to keep scattering losses low. Furthermore, the QPM periods are patterned using standard lithographic means. This allows great flexibility and cost advantages in setting the desired phase-matching wavelength without altering the waveguide structure.

4.2. Development of DD-QPM waveguides

Early work on modulating $\chi^{(2)}$ for AlGaAs-based DD-QPM structures utilized AQWs in the core layer of the waveguide and the symmetry modulation technique. SHG was demonstrated in an AQW waveguide structure in which QWI modulated the $\chi^{(2)}_{zzz}$ tensor element for the $\mathrm{TM_{pump}}\rightarrow\mathrm{TM_{SHout}}$ polarization configuration [23]. However, $\chi^{(2)}_{zzz}$ was found to be weak and the modulation depth small, ultimately leading to poor conversion efficiency. Instead, work on DD-QPM has turned towards the bandgap modulation technique by modifying the large bulk-like $\chi^{(2)}_{zxy}$ tensor element. While modulation of $\chi^{(2)}_{zxy}$ in asymmetric coupled quantum well (ACQW) waveguides was observed [71], it was still too small to be practical. The maximum amount of bandgap shift was limited by both the aluminum mole ratios and thicknesses of the quantum well layers.

In all work that followed, GaAs/AlGaAs superlattices were used instead of ACQWs. The layers of the superlattice were alternated between GaAs and AlAs, the extremity points in aluminum mole ratios for AlGaAs. The periods were also kept short to reduce the diffusion length required during the QWI process. This opened the possibility of fully intermixing the superlattice, a process in which the degree of intermixing is large enough such that the superlattice as a whole reverts to an average alloy of bulk AlGaAs. This potentially provides the maximal amount of shift in the bandgap energy and $\chi^{(2)}$. Calculation of the electronic band structure showed that a short-period symmetric superlattice of 14:14 monolayer GaAs/AlAs provided both a half-bandgap energy near the 1550 nm telecommunications band and a large bandgap energy shift of nearly 25% of the total bandgap energy [72]. Theoretical calculations of $\chi^{(2)}_{zxy}$ for this superlattice showed a potential 35% reduction after intermixing [73], nearly double that measured in ACQWs. In addition, the nonequivalency of the perpendicular and in-plane directions of the superlattice breaks the degeneracy between $\chi^{(2)}_{zxy}$ which is involved in type I phase matching and $\chi^{(2)}_{xyz}$ which is involved in the type II interaction. Predictions place the modulation of $\chi^{(2)}_{xyz}$ at more than twice as large as $\chi^{(2)}_{xyz}$, which leads to potentially greater efficiency.

Initial superlattice DD-QPM waveguides were fabricated using impurity-free vacancy disordering (IFVD) methods for QWI [74]. In IFVD, cap layers of silica were deposited at the surface of the wafer by sputtering. During annealing, defects are formed at the surface due to out-diffusion of gallium atoms into the silica caps. Those defects then diffuse downwards to the superlattice core layer and promote interdiffusion of lattice constituents. Using a superlattice of 14:14 monolayer GaAs/AlAs, QPM gratings were realized by the silica cap method [75]. A photoluminescence peak shift of 45 nm was observed in intermixed regions. Type I SHG was demonstrated using an ultrafast 100 fs laser system operating near 1550 nm. However, second-harmonic powers generated were low, which may be attributed to several factors. Firstly, coupling losses and linear losses of the fundamental wavelength are high which limits the amount of power available for conversion. Secondly, sputtered silica IFVD methods are limited to feature sizes of around 3 μm [76], which is too large considering that the coherence length for three-wave mixing in AlGaAs is of the order of 1.5–2.5 μm depending on the wavelengths. Also, the resolution is highly dependent on how deep the quantum well layers are from the surface. The limited resolution of the silica cap method necessitates the use of third-order QPM gratings which reduces the conversion efficiency. Lastly,

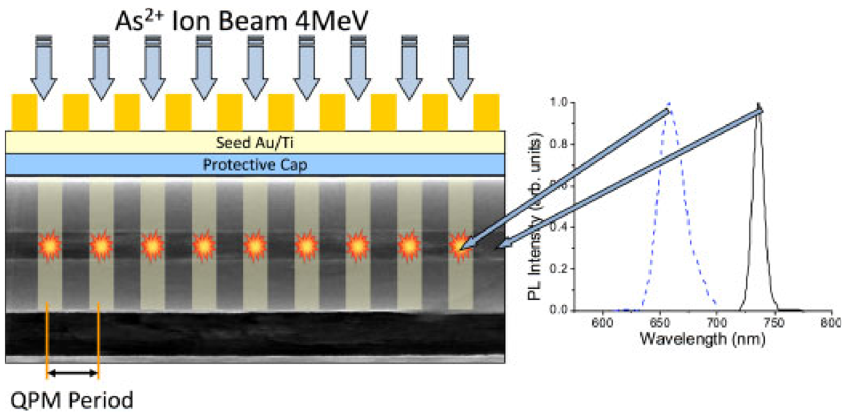

Figure 3 (online color at: www.lpr-journal.org) Schematic cross-section of DD-QPM gratings in a GaAs/AlGaAs superlattice fabricated by patterned ion implantation QWI. Shown are the photoluminescence peaks for as-grown and intermixed domains.

lateral spreading of the defects limit the effective amount of modulation in $\chi^{(2)}$.

In subsequent work, ion implantation-induced disordering (IID) was adopted to create QPM gratings. In this method, As^{2+} ions are implanted directly into the superlattice layer by appropriately setting the ion beam energy. As shown in Fig. 3, ions will pass through windows in a patterned metal implantation mask, leaving some areas disordered and others intact. This form of QWI is superior for several reasons. Firstly, the resolution is significantly greater since defects are formed at the buried superlattice layer itself instead of the surface. This limits lateral diffusion of the defects. Using micro-Raman spectroscopy, it was shown that IID was able to produce the necessary feature sizes for first-order QPM gratings [77]. Secondly, the degree of intermixing can be easily controlled by altering the ion dosage. Lastly, optical losses can be reduced through careful control of the parameters for ion implantation and RTA. However, caution must be exercised to ensure that the implantation process does not cause extended defects or amorphization of the superlattice, which would greatly increase the losses.

Using a similar superlattice-core waveguide structure as before, IID was used to form first-order QPM gratings. Shifts in the bandgap energy of 54 nm after IID were recorded. In nonlinear experiments, output second-harmonic powers exceeded 1 μW for the first time in DD-QPM waveguides and the conversion ratio was tripled over that of previous waveguides made by the silica cap method [78]. However, the conversion efficiency was still limited by the large optical losses (21 dB cm^{-1}) at the fundamental wavelength which were caused by surface damage from etching the gold implantation mask off. Furthermore, the large spectral bandwidth of the 100 fs pulses far exceeded the conversion bandwidth of the QPM grating, thus limiting the amount of SHG possible. In the subsequent generation of devices, an attempt to reduce linear losses was made by adding a protective layer of silicon nitride between the gold implantation mask and the epitaxial layers. Using a 2 ps source, the conversion efficiency was doubled over that of the previous generation [79]. However, difficulties in removing the silicon nitride layers led to significant losses that still limited the SHG process. Also, type II phase matching was not observed, which was likely due to poor confinement of the second-harmonic TE mode in that waveguide design.

4.3. Recent improvements and performance

In more recent devices, a number of improvements have been made. Firstly, the AlAs layers of the superlattice were changed to $Al_{0.85}Ga_{0.15}As$ to avoid oxidation of those layers. We also eliminated a pair of AQWs by terminating the superlattice at either end with barrier layers of $Al_{0.85}Ga_{0.15}As$ instead of well layers of GaAs. This removed a parasitic two-photon absorption peak present in the original wafer design [69]. Secondly, the IID and RTA processes were optimized to provide an appropriate balance between optical losses and bandgap shift. Along with improvements to the reactive ion etching process for forming ridge waveguides, losses were reduced to 5 dB cm^{-1} while increasing the bandgap shift to 76 nm. Thirdly, the waveguides were more deeply etched than previously to provide better confinement of the second harmonic. Using these improvements internal SHG powers of over 9 μW and normalized conversion efficiencies of over 1200 % W^{-1} cm^{-2} for type I phase matching using 2 ps pulses were also produced around 1550 nm. Output second-harmonic powers in excess of 1 μW using a narrow linewidth continuous-wave fundamental source were also produced [67]. The tuning curve of Fig. 4 shows a conversion bandwidth of about 0.4 nm for a 3.5 mm long sample, approximately an order of magnitude smaller than the spectral width of the pulsed laser system. Bistable behavior including hysteresis loops in wavelength tuning and power scans was demonstrated which were attributed to thermal effects from observations of the temporal response of the waveguides.

Recently, type II phase matching was demonstrated in DD-QPM waveguides [80]. Using a 2 ps pulse laser system, the phase-matching wavelengths for several QPM periods were identified, as shown in Fig. 5. The shift in the phase-matching wavelengths relative to the type I process corresponds with the known material birefringence of the superlattice [81]. Output second-harmonic powers of over 2.0 μW and type II conversion efficiencies as high as 350 % W^{-1} cm^{-2} were recorded in a 0.5 mm long sample. At present, type I produces more output second-harmonic power than type II, contrary to our predictions. This is likely due to higher losses in the TE-polarized second harmonic produced in type II and because of group velocity mismatch which is estimated to be larger in type II. It is preferred to

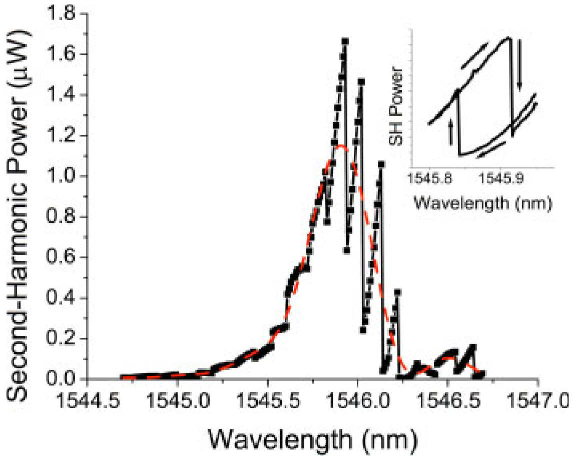

Figure 4 (online color at: www.lpr-journal.org) SHG tuning curves for a DD-QPM waveguide with a 3.5 μm period recorded by scanning a continuous-wave source from short to long wavelengths. The dashed red curve shows the increasing wavelength scan after low pass filtering of the data to remove the Fabry–Pèrot features. The inset shows a tuning hysteresis loop around a single Fabry–Pèrot feature.

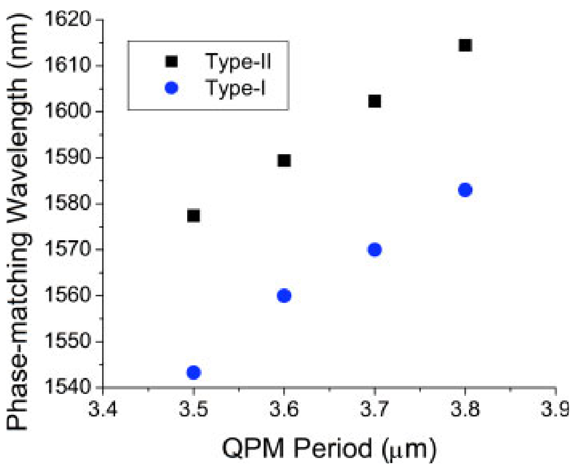

Figure 5 (online color at: www.lpr-journal.org) Phase-matching wavelengths of DD-QPM waveguides with different grating periods for type I and type II processes.

operate the QPM waveguides in the type II configuration for DFG since an on-chip pump laser would naturally emit into the TE polarization.

5. Exact phase matching using Bragg reflection waveguides

Limited progress has been thus far achieved using MPM due to the limitations and severe trade-offs discussed above. A recent design was able to alleviate these trade-offs as well as provide new degrees of freedom using a novel class of MPM. The new approach uses concentric waveguides guiding different light waves using a combination of total internal reflection (TIR) and bandgap effects. This phase-matching technique relies on strong modal dispersion characteristics of Bragg reflection waveguides (BRWs) in conjunction with those of a conventional TIR waveguide within the same structure. These two modes, operating at different wavelengths, can be designed to provide phase matching. This section elucidates the salient properties of BRWs as well as presenting how they can be used to achieve phase matching.

5.1. Bragg reflection waveguides

BRWs are a class of waveguides with leaky, low-loss propagating modes. Through appropriate waveguide design, it is possible to obtain EPM using these waveguides and bypassing the need for a grating to compensate for phase mismatch. A typical slab BRW is composed of a core surrounded by stacks of periodic or quasi-periodic layers on both sides. BRWs have several guiding properties that depart from what is expected from conventional TIR waveguides, which has attracted significant interest [82]. Their unique birefringence properties [83, 84] have been utilized to produce novel devices such as polarization splitters/combiners [85], while their versatile waveguiding properties have been used to tailor the spatial profile of their guided modes [86, 87]. BRWs are also attractive for nonlinear propagation, where spatial optical solitons have been studied [88]. In addition they are useful for applications, where nonlinear optical modes have been found to propagate at higher optical powers in waveguides that do not support propagation of bound modes in the linear regime [89].

Modes that are bound by the reflectivity of Bragg stacks are attractive because their effective indices can be much lower than the material indices of the waveguide constituents. This is in contrast to traditional bounded modes that have modal indices only within the range of constituent material indices. It should be noticed that, although the dominant waveguiding mechanism in BRWs relies on Bragg reflections from periodic claddings, with the proper choice of core and stack indices, TIR modes can also coexist in the structure. In the context of phase matching, this feature was employed to achieve exact MPM of SHG with a pump propagating as TIR mode and the second harmonic propagating as a Bragg mode [20, 90]. Unlike other MPM techniques where phase matching is obtained between high-order modes, BRW phase matching benefits from attaining phase matching between the lowest order modes of the pump and second harmonic, hence maximizing power utilization of both harmonics for the nonlinear interaction.

The quarter-wave BRW (QtW-BRW) is a special case in which the cladding layers have an optical thickness equal to one-quarter of the wavelength with respect to the transverse wave vector. This constraint places the complex Bloch wave number in the middle of the Bragg stopband where its imaginary component has the highest value [82], hence ensuring the most rapid field decay in the claddings. QtW-BRWs are attractive because of their relatively simple design equations which are determined by the quarter-wave condition. A comprehensive analysis of QtW-BRWs can be

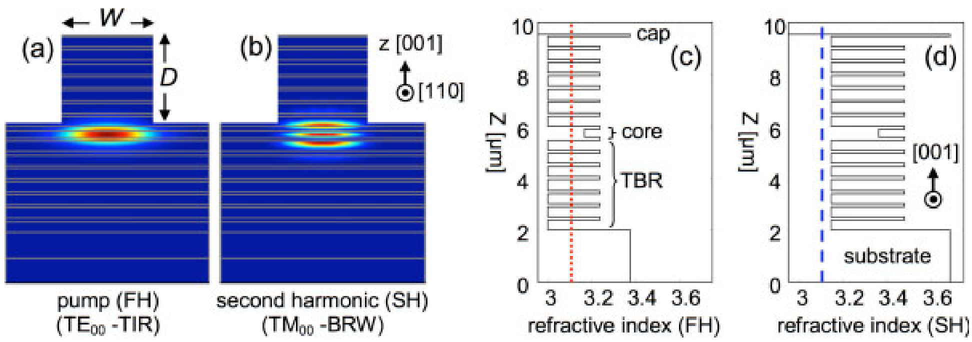

Figure 6 (online color at: www.lpr-journal.org) Schematic of a ridge BRW with ridge width W and etch depth D superimposed by simulated a) intensity profile of TE-polarized pump (FH) and b) intensity profile of TM-polarized second harmonic. c) Index profile at FH frequency and d) index profile at SH frequency. The red dotted line in c) is the effective mode index of the FH and the blue dashed line in d) is that of the SH.

found in [91] where it is proven that the effective index of the fundamental Bragg mode only depends on the operating frequency and the core characteristics and independent of the cladding reflectors. This implies that two different sets of Bragg reflectors can yield the same effective index. This unique feature of QtW-BRWs holds for both TE and TM polarizations of the fundamental Bragg mode and can find potential applications where modal birefringence of orthogonal polarizations is desired to vanish.

5.2. Pulsed and continuous-wave second harmonic generation

There have been several experimental demonstrations of SHG in ridge QtW-BRWs. One recent demonstration involved a two-dimensional QtW-BRW wafer grown on a [001] GaAs substrate using metal–organic chemical vapor deposition (MOCVD) [92]. A representative schematic of the fabricated device along with simulated intensity profiles of the pump and second-harmonic signal, as well as the refractive index profiles at both harmonics are illustrated in Fig. 6. The top and bottom transverse Bragg reflectors consisted of seven periods of $Al_{0.25}Ga_{0.75}As/Al_{0.75}Ga_{0.25}As$ bilayers with associated thicknesses of 123 nm/391 nm. The $Al_{0.40}Ga_{0.60}As$ core had a thickness of 300 nm. The sample was capped with a 50 nm layer of GaAs. Waveguide ridges with widths of 2.5–4.5 µm were patterned through plasma etching for a depth of approximately 3.4 µm to provide lateral confinement.

Characterization of the waveguide linear properties was carried out using the Fabry–Pèrot method. For TE polarization, linear propagation loss was measured as approximately 7.8 cm^{-1}. The input coupling factor was found to be approximately 50%. The characterized sample had a length of 1.96 mm and the ridge waveguide width was 4 µm.

Samples were tested using both pulsed and continuous-wave sources [92]. A tunable pulsed OPO in the frequency range 1500–1600 nm (pulse duration of approximately 2.5 ps and a repetition rate of 76 MHz) was used to characterize the samples. By keeping a constant input

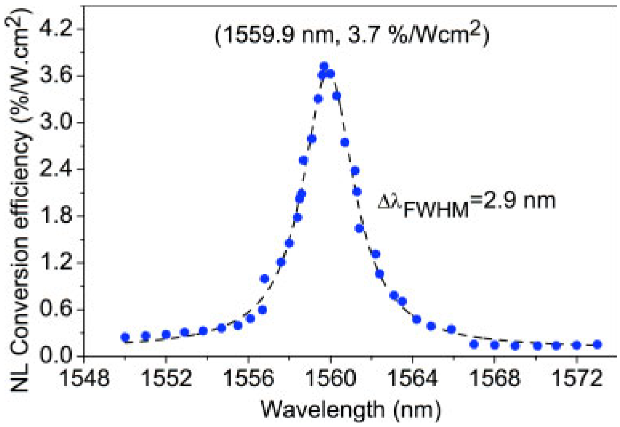

Figure 7 (online color at: www.lpr-journal.org) SHG normalized nonlinear conversion efficiency as a function of pump wavelength (filled circles). The dashed curve is the Lorentzian fit to the measured data. Peak internal second-harmonic power was estimated as 2.4 µW.

power and varying the input fundamental wavelength, the tuning curve of the SHG process was obtained. A maximum second-harmonic power of 2.4 µW was measured at the phase-matching wavelength of $\lambda = 1559.9$ nm. The average internal fundamental power was 41 mW that was maintained at the front facet of the waveguide. The normalized conversion efficiency of the process is illustrated in Fig. 7 where the peak conversion efficiency at 1559.9 nm clearly denotes the TIR to BRW nonlinear conversion mechanism. The maximum conversion efficiency was estimated to be approximately 3.7 % W^{-1} cm^{-2} which is roughly of the same order of magnitude as those of other phase-matching techniques investigated in the literature [93]. Further characterization of the device was carried out with a tunable continuous-wave laser which was amplified using a C-band erbium-doped fiber amplifier. The estimated peak second-harmonic power was 23 nW, which was obtained before the output facet of the waveguide with an internal pump power of $P_\omega \approx 94$ mW estimated after the input facet. The normalized conversion efficiency of the process was estimated to be approximately 6.8×10^{-3} % W^{-1} cm^{-2}.

5.3. Improvements of simple Bragg reflection waveguides

Although phase-matched SHG was observed in QtW-BRWs, the small core dimensions, dictated by the phase-matching condition, limit the efficiency of these devices. A modified BRW design was developed to help alleviate this limitation. This improved structure (BRW-ML) utilized an additional layer, referred to as the matching layer (ML), located between the core and the Bragg reflectors [87, 94]. Inclusion of the ML offers a simple mechanism for aligning the phase of the propagating mode at the boundary between the core and transverse Bragg reflectors. The result is the relaxation of the constraint on the core thickness as well as offering additional flexibility in tailoring the dispersion while maintaining the phase-matching condition.

The index and field profiles of a fabricated BRW-ML [66] along with the previously characterized QtW-BRW [92] are shown in Fig. 8. By comparing the geometries and the field profiles of the two designs, the improvements offered by the BRW-ML can be summarized as: (1) larger core dimension with enhanced confinement; (2) improved overlap factor between the harmonics by reducing the out-of-phase portion of the interacting fields; and (3) locating the peak intensity of the pump (fundamental) within the ML where aluminum concentration is the lowest and $\chi^{(2)}$ coefficient is the largest.

The BRW-ML wafer was grown via MOCVD with the structure optimized for nonlinear overlap factor. Typical propagation losses for TE and TE/TM polarizations were found to be 2.0 and 2.2 cm^{-1}, respectively. A facet reflection coefficient of 29% and an end-fire coupling efficiency of 49% were obtained from the measurements. Characterization of nonlinear properties was carried out using the tunable pulsed OPO source previously discussed in Sect. 4. Both type I and type II interactions were examined. Under an internal input pump power of 3.3 mW, 28 and 60 μW internal SHG at the output facet were obtained for type I and type II processes, respectively. The associated phase-matching wavelengths were 1551 and 1555 nm, respectively. The normalized conversion efficiencies were estimated to be 5.30×10^3 and 1.14×10^4 % W^{-1}cm^{-2} for type I and type II interactions, respectively. Also the measured second-harmonic power and nonlinear conversion efficiency indicated more than an order of magnitude enhancement with respect to the QtW-BRW design in [66]. Moreover, the results obtained here prove the useful power levels of the generated second-harmonic signal and indicate the potential practicality of these devices.

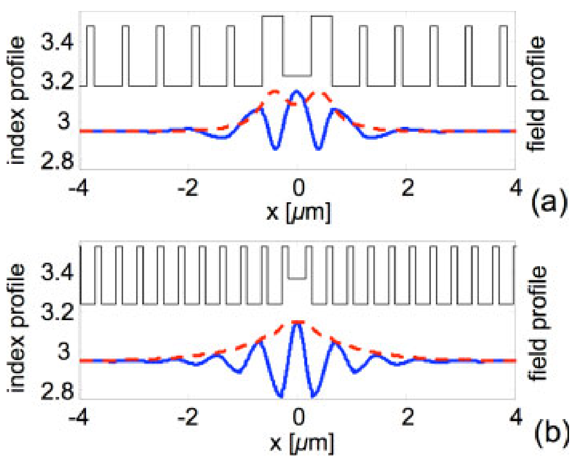

Figure 8 (online color at: www.lpr-journal.org) Field and index profiles of the pump (dashed curve) and second harmonic (solid curve) for a) BRW-ML structure which is characterized in [66] and b) QtW-BRW structure which is characterized in [92]. The core layer is located at $x = 0$ in both figures.

5.4. Applications of dispersion control in phase-matched structures

One of the significant advantages of BRWs in phase matching is the possibility in tailoring the modal dispersion while maintaining phase matching. This enables numerous applications, particularly in the domain of quantum optics, to be implemented in a monolithic platform instead of using bulky optical components. Certain quantum optics applications demand the generation of photon pairs with frequency-entangled properties including generation of frequency correlated, anti-correlated or uncorrelated bi-photons. SPDC in a $\chi^{(2)}$ nonlinear medium is the most widely adopted approach for photon-pair generation. The frequency correlation of photon pairs is primarily determined by the pump bandwidth and the phase-matching condition of the SPDC process. In this regard, dispersion control of the involved harmonics, hence controlling the phase-matching condition, is essential for establishing different schemes of frequency entanglement. In bulk crystals, various techniques have been proposed to control the frequency correlation of photon pairs such as the employment of tilted pulses [95] or chirping the domains of the nonlinearity in QPM configurations [96]. These techniques generally provide control over the frequency–temporal characteristics of photon pairs without offering much flexibility in tailoring their spatiotemporal properties. In contrast, spatial confinement offered by guided-wave structures can improve the spatial characteristics. Moreover, guided-wave structures additionally inherit the waveguide dispersion which has no counterpart in bulk crystals.

BRWs with versatile waveguide dispersion properties deserve some attention as a platform for integrated sources of photon pairs. For ridge BRWs, the effect of waveguide dispersion becomes more pronounced for small ridge widths where optical modes with strong lateral confinement are obtained. In recent work, the influence of the ridge width of an $Al_xGa_{1-x}As$ BRW in controlling the SPDC bandwidth of photon pairs with frequency anti-correlated property was investigated [97]. In that work, it was shown that by simply utilizing waveguides with different ridge widths ranging between 375 and 680 nm and employing type I and type II interactions, SPDC bandwidth tunability in the range 1–450 nm with downconverted photon pairs in the proximity

LASER & PHOTONICS REVIEWS

of the telecommunication spectrum can be achieved. Such flexibility in SPDC bandwidth control for an integrated source of photon pairs can be easily realized by patterning waveguides with different ridge widths through standard lithographic techniques. Investigation of BRW-based integrated photon-pair sources with other frequency correlation properties is currently an ongoing research topic.

6. Progress in monolithic integration

Monolithic integration of active, passive and nonlinear components is one of the main advantages of this phase-matching scheme. The BRW structure is quite capable of all these functions. It should also be noted that this laser structure is identical to that of a vertical cavity surface emitting laser (VCSEL). Such lasers have been well developed over the past three decades. However, in the case discussed here, the Bragg stacks are designed to be quarter-wave for the transverse wave vector and not the full wave vector. By utilizing the technologies developed for VCSELs regarding doping, growth and bandgap engineering, it is possible to design an edge-emitting laser which emits a BRW mode. Such a device can then be monolithically integrated with other BRW sections (nonlinear or passive) for a complete integration platform.

Lasers operating in the BRW mode have been studied theoretically in the past and there can be many benefits. For example, it has been shown that large mode volumes are possible for large core sizes, yet still maintaining a single-mode behaviur [98]. This results in reduced photon density, decreased filamentation and spectral hole burning leading to high power output. It has also been noted that such modes can have higher gain coefficients compared to their conventional counterparts [99]. Further, they also possess strong mode discrimination allowing for stable, single-mode operation. This is due to a large mode spacing and the significant losses of higher order modes [100, 101].

A p–i–n doped wafer was grown using MOCVD with two InGaAs quantum wells in the core region. For an initial demonstration, the structure was grown with a low-index core and thus only supported a BRW mode and no core-confined guided mode. Ridge waveguide lasers etched to a depth of 3.5 μm with ridge widths of 3 μm were fabricated. A representative light–current–voltage curve of the lasers is shown in Fig. 9. For this laser, the turn-on voltage was 1.6 V and the threshold current density was 576 A cm^{-2} for a cavity length of 647 μm. Lower threshold current densities were obtained at longer cavity lengths.

At current densities lower than 10 × threshold, heating effects do not hamper device operation. Spectrally, the laser emission exhibits only one transverse mode. An example is afforded by the inset of Fig. 9 where spectra are shown for 2.5 ×, 5 ×, and 8 × the threshold current value. The wavelength red-shifts at a rate of about 0.1 nm mA^{-1} due to carrier-induced effects. The onset of thermal rollover takes place at approximately 10 × to 15 × the threshold current value. From the figure, the wavelength red-shifts at a rate of about 0.1 nm mA^{-1} but at no point do other

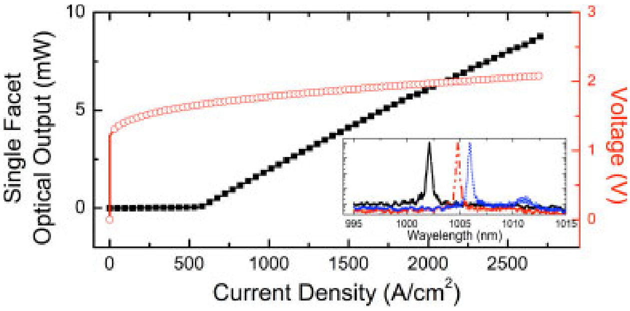

Figure 9 (online color at: www.lpr-journal.org) Typical light–current–voltage curve for a 647 μm cavity length BRW laser. Threshold for this device is 14.8 mA or 576 A cm^{-2} assuming 4 μm lateral width. The inset shows spectra at currents 2.5 × (solid), 5 × (dashed) and 8 × (dotted) above threshold.

transverse modes appear. The emission exhibits a side mode suppression ratio greater than 40 dB for all spectra shown.

Fourier analysis of sub-threshold spectra can give valuable information about a laser [102]. Through this technique, laser characteristics such as modal loss and transparency current density can be determined. A sample sub-threshold spectrum, taken using a high-resolution spectrometer (8 pm resolution), is shown in the inset of Fig. 10. The cavity propagation gain/loss, K, at different sub-threshold currents can be found by analysis of such spectra, as shown in Fig. 10. The current at which $K = 0$ on this curve is the transparency current density. This point is found to be at a value of 409 A cm^{-2}.

The cavity gain/loss data can further be fitted to the following logarithmic relation: $K = G_0 \times \ln(I/I_0) - \alpha_i$. This relates the current to the cavity gain/loss. From this fit, the modal gain parameter is found to be $G_0 = 40.9\,\text{cm}^{-1}$. A modal propagation loss of $\alpha_i = 9\,\text{cm}^{-1}$ was used for this fit. The loss value was obtained using the inverse efficiency technique which characterizes different sample lengths. This range of values was confirmed by another independent technique which compares the internal efficiency at various

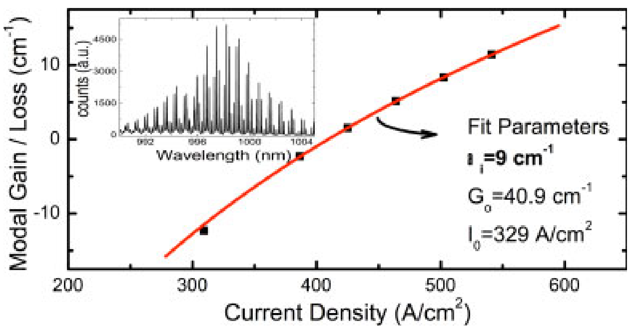

Figure 10 (online color at: www.lpr-journal.org) Cavity propagation gain/loss versus current density of a 647 μm cavity length BRW laser, calculated from Fourier transform analysis of sub-threshold spectra. The data (points) are fit (curve) to the logarithmic equation given in the text. The inset shows the sub-threshold spectrum of a 580 μm cavity length BRW laser operating at 600 A cm^{-2} (14 mA).

temperatures. This is the first determination of low-loss propagation of a BRW photonic bandgap mode, and such structures are indeed suitable for monolithic integration of passive, active and nonlinear components. Through phase matching of this electrically generated BRW mode and other TIR modes or other BRW modes, next-generation integrated nonlinear devices can be realized.

7. Summary

Phase-matching techniques for second-order nonlinearities in semiconductor waveguides were reviewed. QPM via domain disordering utilizing QWI and EPM using BRWs were discussed.

Significant progress has been demonstrated for QPM using domain disordering. Many fabrication challenges have been solved leading to a reduction in losses to around $1\,\mathrm{cm}^{-1}$. Also waveguide design improvements have led to better confinement and enhanced efficiency to $1200\,\%\,\mathrm{W}^{-1}\,\mathrm{cm}^{-2}$.

The versatility of the technique in allowing lithographic inclusion of numerous periods on a single chip lends itself to numerous applications. For instance, several integrated OPO devices may be placed on the same chip with each having a different QPM period to cover different spectral bands. This would allow for broadband spectroscopy in a compact device suitable for portable sensors. Also, broad conversion bandwidths can be achieved in a single chirped QPM grating. Current challenges that need to be addressed include reducing waveguide losses at the pump wavelengths, thermal stability, dealing with higher order nonlinear effects and improving the nonlinear conversion strength through improved waveguide architecture.

It has also been demonstrated that BRWs are powerful phase-matching systems, where semiconductors are dispersive. The ability to tune pertinent parameters, including overlap between the modal profiles of the interacting waves, bandgap, losses, group velocity mismatch (GVM) and group velocity dispersion (GVD), enables performance optimization. BRWs can not only obtain phase matching for any Al percentage and any bandgap desired, but also optimize the GVM and GVD along with the overlap between the modal profiles of the interacting waves which relates the effective second-order nonlinear coefficient.

Another particular strength of the relative efficiency of EPM using BRWs is that their polarization selection rules govern the applications within which they are used. In generating frequency-entangled photon pairs for SPDC, the phase-matching type governs the polarization state of the downconverted photons. Having versatile and tunable polarization properties while maintaining phase matching would further enrich the capabilities and functionality obtained by using the $\chi^{(2)}$ nonlinearity of the GaAs/Al$_x$Ga$_{1-x}$As system in classical and nonclassical applications.

The developments discussed above hold significant promise for integrated, monolithic devices which incorporate second-order nonlinearities. These will serve as a cornerstone of a new class of photonic devices, which utilize powerful ultrafast parametric effects. In turn this will lead to new functionality that will increase the use of photonics in a wider range of practical applications.

Received: 13 April 2010, **Revised:** 20 July 2010, **Accepted:** 9 August 2010

Published online: 20 September 2010

Key words: Phase matching, second-order nonlinearities, semiconductor waveguides, optical parametric processes, optical nonlinearities, second harmonic generation, frequency mixing, monolithic integration of nonlinear structures.

Amr Helmy is an Associate Professor in the department of ECE at the University of Toronto. Prior to his academic career, he held a position at Agilent Technologies in the UK between 2000 and 2004. He received his Ph. D. and M. Sc. from the University of Glasgow, in 1999 and 1994 respectively. He received his B. Sc. from Cairo University in 1993.

Payam Abolghasem received the B. A. Sc. in Electrical Engineering from University of Ottawa, Canada, in 2004 and the M. A. Sc. from McMaster University, Hamilton, Canada, in 2006. He is currently studying toward his Ph. D. degree in University of Toronto, Canada, in the Edward S. Rogers Sr. Department of Electrical and Computer Engineering. His research interests are in optical nonlinear frequency mixing, all-semiconductor integrated parametric devices and infrared optoelectronics.

J. Stewart Aitchison received his B. Sc. and Ph. D. from the Heriot-Watt University in 1984 and 1987, respectively. In 1990 he joined the Department of Electrical and Computer Engineering, University of Glasgow where he became Professor of Photonics in 1999 and holder of the Nortel Institute chair in Emerging Technology in 2001. From 2004 to 2007 he was the director of the Emerging Communications Technology Institute (ECTI) and since 2007 has been vice Dean for Research in the Faculty of Applied Science and Engineering.

Bhavin J. Bijlani graduated in Engineering Science at the University of Toronto in 2005 where he currently is completing his Ph. D. in the photonics group of the Electrical and Computer Engineering Department. His research is in nonlinear frequency conversion and diode lasers in semiconductor Bragg Reflection Waveguides.

Junbo Han received both his B. A. Sc. (2002) and Ph. D. (2007) from Wuhan University, P. R. China. His main experiences were concerned with the preparation of nanostructures (nano-wires, nano-rods, and nano-composite) and the investigation of their nonlinear optical properties. He is now a postdoctoral fellow in the photonics group of University of Toronto. His research interests include photonic device physics, nonlinear optics, and novel nano-structures.

Barry Holmes obtained his Ph. D. from the Coventry University in 2000. After two years as a Scientific Consultant at the

Surface Technology Systems Plc. in Newport, South Wales, he joined the Opto-Electronics Research Group at the University of Glasgow in 2003, where he currently holds the position of Senior Research Fellow. His research interests include integrated optical, magneto-optical and optoelectronic systems, photonic integrated circuits, non-linear optical systems and quantum cascade devices.

David C. Hutchings is a world leading expert on nonlinear optics and optoelectronic integration in semiconductors and was appointed to a personal chair in Optical and Quantum Electronics at the University of Glasgow in 2004. He obtained his Ph. D. from Heriot-Watt University in 1988. Following postdoctoral appointments at Heriot-Watt Univ. and at CREOL, Univ. of Central Florida, he held fellowships at the University of Glasgow from the Royal Society of Edinburgh/Scottish Office or Executive (1992–1995, 2003) and EPSRC (1995–2000).

Usman Younis received his BE-Computer Software and MS-Information Technology degrees from National University of Sciences and Technology, Islamabad, Pakistan, in 2004 and 2006. He joined University of Glasgow, UK, in 2007, where he completed his Ph. D. in Electronics and Electrical Engineering in 2010. He has been actively involved in III-V fabrication technologies, integrated optoelectronics, laser physics, and applied non-linear optics.

Sean J. Wagner obtained his B. A. Sc. degree in Computer Engineering at the University of Waterloo in 2003 and his M. A. Sc. degree in Electrical Engineering from the University of Toronto in 2006. He has previously held positions at IBM, Royal Philips Electronics, and Evertz Microsystems. In his doctoral research at the University of Toronto, Sean is investigating all-optical wavelength conversion devices based semiconductor superlattices and monolithic integration techniques. His other research interests include semiconductor nanofabrication, photonic integrated circuits, all-optical interconnect, and organic optoelectronics.

References

[1] P. A. Franken, A. E. Hill, C. W. Peters, and G. Weinrich, Phys. Rev. Lett. **7**(4), 118–120 (1961).
[2] J. A. Armstrong, N. Bloembergen, J. Ducuing, and P. S. Pershan, Phys. Rev. **127**(6), 1918–1939 (1962).
[3] M. M. Fejer, G. A. Magel, D. H. Jundt, and R. L. Byer, IEEE J. Quantum Electron. **28**(11), 2631–2654 (1992).
[4] Y. S. Liu, D. Dentz, and R. Belt, Opt. Lett. **9**(3), 76–78 (1984).
[5] K. Kato, IEEE J. Quantum Electron. **22**(7), 1013–1014 (1986).
[6] L. E. Myers, R. C. Eckardt, M. M. Fejer, R. L. Byer, W. R. Bosenberg, and J. W. Pierce, J. Opt. Soc. Am. B **12**(11), 2102–2116 (1995).
[7] J. D. Bierlein and H. Vanherzeele, J. Opt. Soc. Am. B **6**(4), 622–633 (1989).
[8] U. Heitmann, M. Kötteritzsch, S. Heitz, and A. Hese, Appl. Phys. B **55**, 419–423 (1992).
[9] H. P. Wagner, Phys. Stat. Sol. B **187**, 363–369 (1995).
[10] H. P. Wagner, S. Wittmann, H. Schmitzer, and H. Stanzl, J. Appl. Phys. **77**(8), 3637–3640 (1995).
[11] S. Janz, C. Fernando, H. Dai, F. Chatenoud, M. Dion, and R. Normandin, Opt. Lett. **18**(8), 589–591 (1993).
[12] M. Cada, M. Svilans, S. Janz, R. Bierman, R. Normandin, and J. Glinski, Appl. Phys. Lett. **61**(17), 2090–2092 (1992).
[13] J. H. Marsh, Semicond. Sci. Technol. **8**, 1136–1155 (1993).
[14] B. Ryvkin, K. Panajotov, A. Georgievski, J. Danckaert, M. Peeters, G. Verschaffelt, H. Thienpont, and I. Veretennicoff, J. Opt. Soc. Am. B **16**(11), 2106–2113 (1999).
[15] A. Tredicucci, C. Gmachl, F. Capasso, D. L. Sivco, A. L. Hutchinson, and A. Y. Cho, Appl. Phys. Lett. **74**(5), 638–640 (1999).
[16] N. Nunoya, M. Nakamura, M. Morshed, S. Tamura, and S. Arai, IEEE J. Sel. Top. Quantum Electron. **7**(2), 249–258 (2001).
[17] M. Aoki, M. Suzuki, H. Sano, T. Kawano, T. Ido, T. Taniwatari, K. Uomi, and A. Takai, IEEE J. Quantum Electron. **29**(6), 2088–2096 (1993).
[18] P. Doussiere, P. Garabedian, C. Graver, D. Bonnevie, T. Fillion, E. Derouin, M. Monnot, J. G. Provost, D. Leclerc, and M. Klenk, IEEE Photon. Technol. Lett. **6**(2), 170–172 (1994).
[19] T. L. Koch and U. Koren, IEEE J. Quantum Electron. **27**(3), 641–653 (1991).
[20] A. S. Helmy, Opt. Express **14**(3), 1243–1252 (2006).
[21] M. M. Choy and R. L. Byer, Phys. Rev. B **14**(4), 1693–1706 (1976).
[22] E. . Sipe, D. J. Moss, and H. M. van Driel, Phys. Rev. B **35**(1), 1129–1141 (1987).
[23] J. P. Bouchard, M. Tetu, S. Janz, D. X. Xu, Z. R. Wasilewski, P. Piva, U. G. Akano, and I. V. Mitchell, Appl. Phys. Lett. **77**(26), 4247–4249 (2000).
[24] K. Moutzouris, S. V. Rao, M. Ebrahimzadeh, A. D. Rossi, V. Berger, M. Calligaro, and V. Ortiz, Opt. Lett. **26**(22), 1785–1787 (2001).
[25] A. Fiore, V. Berger, E. Rosencher, P. Bravetti, and J. Nagle, Nature **391**, 463–466 (1998).
[26] A. De Rossi, V. Berger, M. Calligaro, G. Leo, V. Ortiz, and X. Marcadet, Appl. Phys. Lett. **79**(23), 3758–3760 (2001).
[27] L. Scaccabarozzi, M. M. Fejer, Y. Huo, S. Fan, X. Yu, and J. S. Harris, Opt. Lett. **31**(24), 3626–3628 (2006).
[28] E. Guillotel, M. Ravaro, F. Ghiglieno, C. Langlois, C. Ricolleau, S. Ducci, I. Favero, and G. Leo, Appl. Phys. Lett. **94**(17), 171110 (2009).
[29] K. Moutzouris, S. V. Rao, M. Ebrahimzadeh, A. De Rossi, M. Calligaro, V. Ortiz, and V. Berger, Appl. Phys. Lett. **83**(4), 620–622 (2003).
[30] S. Ducci, L. Lanco, V. Berger, A. De Rossi, V. Ortiz, and M. Calligaro, Appl. Phys. Lett. **84**(16), 2974–2976 (2004).
[31] S. J. B. Yoo, R. Bhat, C. Caneau, and M. A. Koza, Appl. Phys. Lett. **66**, 3410–3412 (1995).
[32] S. J. B. Yoo, C. Caneau, R. Bhat, M. A. Koza, A. Rajhel, and N. Antoniades, Appl. Phys. Lett. **68**(19), 2609–2611 (1996).
[33] X. Yu, L. Scaccobarozzi, J. S. Harris Jr., P. S. Kuo, and M. M. Fejer, Opt. Express **13**(26), 10742–10748 (2005).
[34] T. Skauli, K. L. Vodopyanov, T. J. Pinguet, A. Schober, O. Levi, L. A. Eyres, M. M. Fejer, J. S. Harris, B. Gerard, L. Becouarn, E. Lallier, and G. Arisholm, Opt. Lett. **27**(8), 628–630 (2002).

[35] P.S. Kuo, K.L. Vodopyanov, M.M. Fejer, D.M. Simanovskii, X. Yu, J.S. Harris, D. Bliss, and D. Weyburne, Opt. Lett. **31**(1), 71–73 (2006).
[36] J. Schaar, K. Vodopyanov, P. Kuo, M. Fejer, X. Yu, A. Lin, J. Harris, D. Bliss, C. Lynch, V. Kozlov, and W. Hurlbut, IEEE J. Sel. Top. Quantum Electron. **14**(2), 354–362 (2008).
[37] J. Ota, W. Narita, I. Ohta, T. Matsushita, and T. Kondo, Jpn. J. Appl. Phys. **48**(4), 04C110 (2009).
[38] X.J. Yu, L. Scaccabarozzi, A.C. Lin, J.X. Fu, P.S. Kuo, M.M. Fejer, and J.S. Harris, Proc. SPIE **6103**, 61030N (1992).
[39] X.J. Yu, L. Scaccabarozzi, A.C. Lin, M.M. Fejer, and J.S. Harris, J. Cryst. Growth **301–302**, 163–167 (2007).
[40] K.L. Vodopyanov, O. Levi, P.S. Kuo, T.J. Pinguet, J.S. Harris, M.M. Fejer, B. Gerard, L. Becouarn, and E. Lallier, Opt. Lett. **29**(16), 1912–1914 (2004).
[41] P.S. Kuo, K.L. Vodopyanov, M.M. Fejer, X. Yu, J.S. Harris, and D. Weyburne, Opt. Lett. **32**(18), 2735–2737 (2007).
[42] P.S. Kuo, K.L. Vodopyanov, M.M. Fejer, X. Yu, J.S. Harris, D.M. Simanovskii, D. Bliss, and D. Weyburne, Mid-IR Continuum from an Optical Parametric Generator based on Orientation-Patterned GaAs (OP-GaAs), paper CWE1, in: Proceedings of the Conference on Lasers and Electro-Optics (CLEO) (Tech. Digest, Vol. 2, Optical Society of America, 2005), pp. 1294–1296.
[43] K.L. Vodopyanov, Laser Photon. Rev. **2**(1–2), 11–25 (2008).
[44] E.U. Rafailov, P. Loza-Alvarez, C.T.A. Brown, W. Sibbett, R.M. De La Rue, P. Millar, D.A. Yanson, J.S. Roberts, and P.A. Houston, Opt. Lett. **26**(24), 1984–1986 (2001).
[45] S. Nakagawa, N. Yamada, N. Mikoshiba, and D.E. Mars, Appl. Phys. Lett. **66**(17), 2159–2161 (1995).
[46] C. Simonneau, J.P. Debray, J.C. Harmand, P. Vidakovic, D.J. Lovering, and J.A. Levenson, Opt. Lett. **22**(23), 1775–1777 (1997).
[47] M. Scalora, M.J. Bolemer, A.S. Manka, J.P. Dowling, C.M. Bowden, R. Viswanathan, and J.W. Haus, Phys. Rev. A **56**(4), 3166–3174 (1997).
[48] M. Centini, C. Sibilia, M. Scalora, G. D'Aguanno, M. Bertolotti, M.J. Bloemer, C.M. Bowden, and I. Nefedov, Phys. Rev. E **60**(4), 4891–4898 (1999).
[49] C. De Angelis, F. Gringoli, M. Midrio, D. Modotto, J.S. Aitchison, and G.F. Nalesso, J. Opt. Soc. Am. B **18**(3), 348–351 (2001).
[50] Y. Dumeige, I. Sagnes, P. Monnier, P. Vidakovic, I. Abram, C. Meriadec, and A. Levenson, Phys. Rev. Lett. **89**(4), 043901 (2002).
[51] G.T. Kiehne, A.E. Kryukov, and J.B. Ketterson, Appl. Phys. Lett. **75**(12), 1676–1678 (1999).
[52] M. Centini, G. D'Aguanno, L. Sciscione, C. Sibilia, M. Bertolotti, M. Scalora, and M.J. Bloemer, Opt. Lett. **29**(6), 1924–1926 (2004).
[53] Y. Dumeige, P. Vidakovic, S. Sauvage, I. Sagnes, J.A. Levenson, C. Sibilia, M. Centini, G. D'Aguanno, and M. Scalora, Appl. Phys. Lett. **78**(20), 3021–3023 (2001).
[54] G. D'Aguanno, M. Centini, M. Scalora, C. Sibilia, Y. Dumeige, P. Vidakovic, J.A. Levenson, M.J. Bloemer, C.M. Bowden, J.W. Haus, and M. Bertolotti, Phys. Rev. E **64**, 016609 (2001).
[55] M. Liscidini and L.C. Andreani, Appl. Phys. Lett. **85**(11), 1883–1885 (2005).
[56] M. Liscidini and L.C. Andreani, Phys. Rev. E **73**, 016613 (2006).
[57] M. Liscidini, A. Locatelli, L.C. Andreani, and C. De Angelis, Phys. Rev. Lett. **99**, 053907 (2007).
[58] J. Martorell and R. Corbalan, Opt. Commun. **108**, 319–323 (1994).
[59] J. Trull and R. Corbalan, Opt. Lett. **20**(17), 1746–1748 (1995).
[60] J. Martorell, R. Vilaseca, and R. Corbalan, Appl. Phys. Lett. **70**(6), 702–704 (1997).
[61] A. Yariv and P. Yeh, J. Opt. Soc. Am. B **67**, 438–448 (1977).
[62] A.R. Cowan and J.F. Young, Phys. Rev. B **65**, 085106 (2002).
[63] A.M. Malvezzi, G. Vecchi, M. Patrini, G. Guizzetti, L.C. Andreani, F. Romanato, L. Businaro, E. Di Fabrizio, A. Passaseo, and M. De Vittorio, Phys. Rev. B **68**, 161306(R) (2003).
[64] E. Centeno, D. Felbacq, and D. Cassagne, Phys. Rev. Lett. **98**, 263903 (2007).
[65] A. Fiore, S. Janz, L. Delobel, P. van der Meer, P. Bravetti, V. Berger, E. Rosencher, and J. Nagle, Appl. Phys. Lett. **72**(23), 2942–2944 (1998).
[66] P. Abolghasem, J. Han, B.J. Bijlani, A. Arjmand, and A.S. Helmy, IEEE Photon. Technol. Lett. **21**(19), 1462–1464 (2009).
[67] S.J. Wagner, B.M. Holmes, U. Younis, A.S. Helmy, J.S. Aitchison, and D.C. Hutchings, Appl. Phys. Lett. **94**(15), 151107 (2009).
[68] J.H. Marsh, Semicond. Sci. Technol. **6**, 1136–1155 (1993).
[69] S.J. Wagner, B.M. Holmes, U. Younis, A.S. Helmy, D.C. Hutchings, and J.S. Aitchison, IEEE Photon. Technol. Lett. **21**(2), 85–87 (2009).
[70] B.S. Ooi, K. McIlvaney, M.W. Street, A.S. Helmy, S.G. Ayling, A.C. Bryce, J.H. Marsh, and J.S. Roberts, IEEE J. Quantum Electron. **33**(10), 1784–1793 (1997).
[71] J.S. Aitchison, M.W. Street, N.D. Whitbread, D.C. Hutchings, J.H. Marsh, G.T. Kennedy, and W. Sibbett, IEEE J. Sel. Top. Quantum Electron. **4**(4), 695–700 (1998).
[72] D.C. Hutchings and T.C. Kleckner, J. Opt. Soc. Am. B **19**(4), 890–894 (2002).
[73] D. Hutchings, IEEE J. Sel. Top. Quantum Electron. **10**(5), 1124–1132 (2004).
[74] A.S. Helmy, N.P. Johnson, M.L. Ke, A.C. Bryce, J.S. Aitchison, J.H. Marsh, I. Gontijo, G.S. Buller, J. Davidson, and P. Dawson, IEEE J. Sel. Top. Quantum Electron. **4**(4), 661–668 (1998).
[75] A.S. Helmy, D.C. Hutchings, T.C. Kleckner, J.H. Marsh, A.C. Bryce, J.M. Arnold, C.R. Stanley, J.S. Aitchison, C.T.A. Brown, K. Moutzouris, and M. Ebrahimzadeh, Opt. Lett. **25**(18), 1370–1372 (2000).
[76] A.S. Helmy, A.C. Bryce, D.C. Hutchings, J.S. Aitchison, and J.H. Marsh, J. Appl. Phys. **100**(12), 123107 (2006).
[77] P. Scrutton, M. Sorel, D.C. Hutchings, J.S. Aitchison, and A.S. Helmy, IEEE Photon. Technol. Lett. **19**(9), 677–679 (2007).
[78] K. Zeaiter, D.C. Hutchings, R.M. Gwilliam, K. Moutzouris, S.V. Rao, and M. Ebrahimzadeh, Opt. Lett. **28**(11), 911–913 (2003).
[79] D.C. Hutchings, M. Sorel, K. Zeaiter, A.J. Zilkie, B. Leesti, A.S. Helmy, P.W.E. Smith, and J.S. Aitchison, Proceedings Nonlinear Guided Waves (OSA, Toronto, Canada, 2004).
[80] B.M. Holmes, U. Younis, D.C. Hutchings, S.J. Wagner, A.S. Helmy, and J.S. Aitchison, Proceedings Conference on Lasers and Electro-Optics (OSA, Baltimore, MD, 2009).

[81] T. C. Kleckner, A. S. Helmy, K. Zeaiter, D. C. Hutchings, and J. S. Aitchison, IEEE J. Quantum Electron. **42**(3), 280–286 (2006).
[82] P. Yeh and A. Yariv, Opt. Commun. **19**(3), 427–430 (1976).
[83] P. Yeh, A. Yariv, and C. S. Hong, J. Opt. Soc. Am. **67**(4), 423–438 (1977).
[84] S. R. A. Dods, J. Opt. Soc. Am. A **6**(9), 1465–1476 (1989).
[85] E. Simova and I. Golub, Opt. Express **11**(25), 3425–3430 (2003).
[86] A. Mizrahi and L. Schächter, Phys. Rev. E **70**(1), 016505 (2004).
[87] A. Mizrahi and L. Schächter, Opt. Express **12**(14), 3156–3170 (2004).
[88] C. Wächter, F. Lederer, L. Leine, U. Trutschel, and M. Mann, J. Appl. Phys. **71**(8), 3688–3692 (1992).
[89] P. M. Lambkin and K. A. Shore, IEEE J. Sel. Top. Quantum Electron. **27**(3), 824–829 (1991).
[90] A. S. Helmy, B. Bijlani, and P. Abolghasem, Opt. Lett. **32**(16), 2399–2401 (2007).
[91] B. R. West and A. S. Helmy, J. Opt. Soc. Am. B **23**(6), 1207–1220 (2006).
[92] P. Abolghasem, J. Han, B. J. Bijlani, A. Arjmand, and A. S. Helmy, Opt. Express **17**(11), 9460–9467 (2009).
[93] S. V. Rao, K. Moutzouris, and M. Ebrahimzadeh, J. Opt. A, Pure Appl. Opt. **6**(6), 569–584 (2004).
[94] P. Abolghasem and A. S. Helmy, IEEE J. Quantum Electron. **45**(6), 646–653 (2009).
[95] M. Hendrych, M. Mičuda, and J. P. Torres, Opt. Lett. **32**(16), 2339–2341 (2007).
[96] M. B. Nasr, S. Carrasco, B. A. E. Saleh, A. V. Sergienko, M. C. Teich, J. P. Torres, L. Torner, D. S. Hum, and M. M. Fejer, Phys. Rev. Lett. **100**(18), 183601 (2008).
[97] P. Abolghasem, M. Hendrych, X. Shi, J. P. Torres, and A. S. Helmy, Opt. Lett. **34**(13), 2000–2002 (2009).
[98] T. H. Her, Opt. Express **16**(10), 7197–7202 (2008).
[99] A. Yariv, Y. Xu, and M. Shayan, Opt. Lett. **28**(3), 176–178 (2003).
[100] L. Zhu, A. Scherer, and A. Yariv, IEEE J. Quantum Electron. **43**(10), 934–940 (2007).
[101] A. Mock, L. Lu, E. H. Hwang, J. O'Brien, and P. D. Dapkus, IEEE J. Sel. Top. Quantum Electron. **15**(3), 892–900 (2009).
[102] D. Hofstetter and R. L. Thornton, IEEE J. Quantum Electron. **34**(10), 1914–1923 (1998).